

# Single Shot Lensless Interferenceless Phase Imaging of Biochemical Samples Using Synchrotron Near Infrared Beam

Molong Han<sup>a\*</sup>, Daniel Smith<sup>a\*</sup>, Soon Hock Ng<sup>a</sup>, Tomas Katkus<sup>a</sup>, Aravind Simon John Francis Rajeswary<sup>b</sup>, Periyasamy Angamuthu Praveen<sup>b</sup>, Keith R. Bambery<sup>c</sup>, Mark J. Tobin<sup>c</sup>, Jitraporn Vongsvivut<sup>c</sup>, Saulius Juodkazis<sup>a,d</sup>, Vijayakumar Anand<sup>a,b</sup>

<sup>a</sup>Optical Sciences Centre and ARC Training Centre in Surface Engineering for Advanced Materials (SEAM), School of Science, Swinburne University of Technology, Hawthorn, VIC 3122, Australia;

<sup>b</sup>Institute of Physics, University of Tartu, W. Ostwaldi 1, 50411 Tartu, Estonia; <sup>c</sup>Infrared

Microspectroscopy (IRM) Beamline, ANSTO—Australian Synchrotron, Clayton, VIC 3168,

Australia; <sup>d</sup>Tokyo Tech World Research Hub Initiative, School of Materials and Chemical Technology, Tokyo Institute of Technology, 2-12-1, Ookayama, Meguro-ku, Tokyo 152-8550, Japan

## ABSTRACT

Near-IR (NIR) region of the synchrotron-IR beam, which is usually filtered out in order to improve the signal to noise ratio of Fourier-transform infrared spectroscopy (FTIR), was extracted and used as an illuminating source to achieve phase imaging of biochemical samples. A 200-um pinhole was aligned with one lobe of the unique fork shaped NIR synchrotron beam at a resulting intensity maximum. The diffracted light with airy diffraction pattern passed the biochemical sample and was collected by NIR sensitive lensless camera. The Gerchberg-Saxton algorithm (GSA) was used to reconstruct the phase images of the samples from recorded the intensity images.

**Keywords:** phase imaging, bioimaging, synchrotron, near infrared beam, holography, incoherent optics, chemical imaging, phase retrieval, 3D imaging

## 1. INTRODUCTION

Recently, novel imaging techniques have been employed beyond the physical boundaries at IRM beamline of Australian Synchrotron [1-3]. A single shot 3D semi-synthetic imaging technique has been demonstrated using focal plane array imaging detector of FTIR with offline radiation source [1]. It is challenging to achieve this imaging technique using synchrotron radiation source since the synchrotron beam has a unique fork-shape intensity distribution. Additionally, as synchrotron radiation source contains both linear and circular polarizations as well as spatial and temporal incoherence, interference-based approach would impose unpredicted responses [4]. Therefore, there is a need to extract phase information of samples without employing lenses and interference. A recent study has shown using a single refractive lens without two beam interferences for 3D imaging with a single camera shot [5]. Thus, we believe that the proposed method benefited from fast phase-retrieval algorithm has the potential to achieve interference-free 3D phase imaging without employing lenses.

## 2. MATERIALS AND METHODS

The figure 1(a) shows the schematic of the optical configuration of phase imaging module using NIR synchrotron beamline. The IR beam extracted from synchrotron source went through a low wavelength filter, where only NIR beam can pass through. The NIR beam aligned with a 200um pinhole to create airy pattern illumination at a maximum intensity. This airy pattern light was illuminated on the sample and detected by a lensless NIR sensitive camera (Canon EOS 6D). The complex amplitude at  $z_1$  distance from pinhole can be obtained as  $C_1\sqrt{I_0}Q(1/z_1)$ , where  $z_1$  is the distance between the pinhole and the specimen plane,  $C_1$  is a complex constant and  $Q(a)$  is equal to  $\exp[j\pi aR^2/\lambda]$ . The complex

amplitude at specimen plane can be given as  $C_2\sqrt{I_0}Q(1/z_1)\exp[-j\Phi_s(x,y)]$ , where  $C_2$  is a complex constant,  $\Phi_s(x,y)$  is the phase difference caused by the specimen where  $\Phi_s(x,y) = \frac{2\pi t(x,y)}{\lambda} [n(x,y) - 1]$ . The intensity at detector plane is given by convolution of the complex amplitude at specimen plane and the propagator between specimen plane and detector plane as  $I_s = |C_2\sqrt{I_0}Q(1/z_1)\exp[-j\Phi_s(x,y)]\otimes Q(1/z_2)|^2$ .

The intensity information at specimen plane is available as a constant while the intensity information at the detector plane is obtained by direct measurement. The phase information can be estimate using the GSA [6-9]. The figure 1(b) shows the phase image reconstruction procedure from intensity images using the phase-retrieval algorithm.  $\psi_1$  and  $\psi_2$  are the complex amplitude at detector plane and specimen plane respectively, in which the phase variables at these two planes are unknown. Initially, assuming phase variable is zero at detector plane, the complex amplitude  $\psi_1$  can be simply expressed as  $\sqrt{I_s}$  (phase = 0). The complex amplitude at specimen plane  $\psi_2$  can be obtained by convolution of  $\psi_1$  and a forward spherical propagator as  $\psi_2 = S^-(z)\otimes\sqrt{I_s}$ , where the forward spherical propagator is given as  $S^-(z) = \exp[-j2\pi R/\lambda]$ . Due to the phase variable is unknown, the complex amplitude at specimen plane  $\psi_2$  can be rewritten as  $\psi_2 = \sqrt{I_0}\cdot\exp[j(\arg\{S^-(z)\otimes\sqrt{I_s}\})]$ . The convolution of specimen plane  $\psi_2$  and a backward propagator  $S^+(z) = \exp[j2\pi R/\lambda]$  gives the complex amplitude at detector plane  $\psi_1$ , which can be expressed as  $\psi_1 = \{\sqrt{I_0}\cdot\exp[j(\arg\{S^-(z)\otimes\sqrt{I_s}\})]\}\otimes S^+(z)$ . And then at detector plane, intensity variable is replaced by measured intensity  $\sqrt{I_s}$  and the phase variable is retained. The process will be repeated until a good estimation of the phase image.

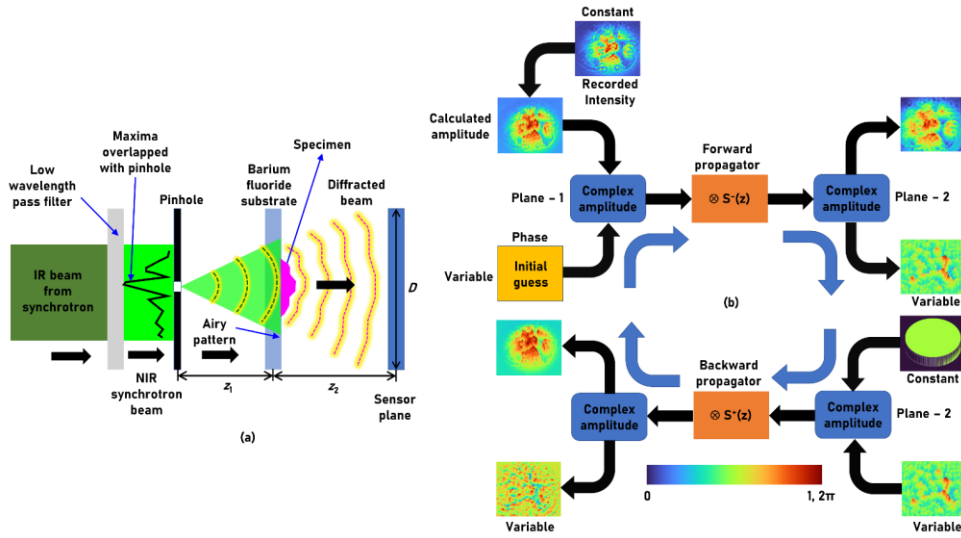


**Figure 1.** (a) Schematic of the optical configuration. (b) Phase-retrieval algorithm with spherical propagator for estimation of phase at plane 2 from the intensity at plane 1.

### 3. RESULTS AND DISCUSSION

Two samples were prepared for the phase imaging experiment. In the first sample, 15um-diameter latex beads were randomly arranged on a barium fluoride substrate. The sample was placed with a sample-to-pinhole distance of 50 cm and a sample-to-camera distance of 7 cm. The phase retrieval algorithm was repeated four times to estimate the phase image. Figure 2(a)-(e) shows recorded intensity image, rescaled intensity image, reconstructed phase image using GSA after two repeats, optical image, and the estimated phase image, respectively. Comparing figure 2(d) and (e), the bead area shows an approximately a  $\pi$  shift in phase comparing with no-bead area, which is consistent with the optical image.

However, the resolution of the phase image is lower than the optical image, which is resulted from large wavelength of illumination source and low spatial coherence and numerical aperture of this imaging system.

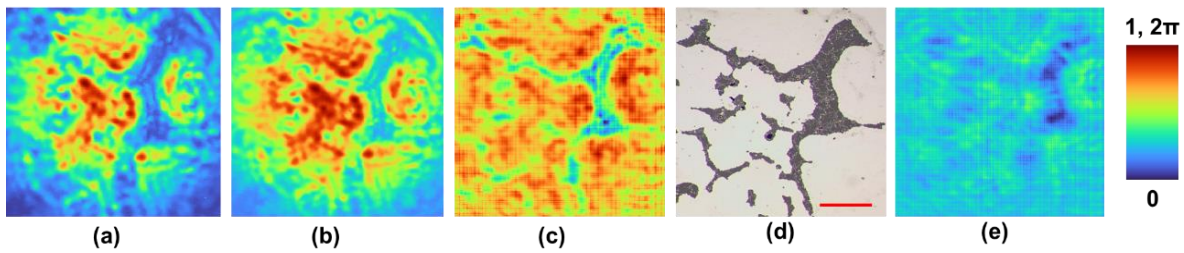


**Figure 2.** (a) Recorded intensity distribution for the latex beads ( $\sim 15 \mu\text{m}$  in diameter). (b) Calculated amplitude of the recorded intensity distribution. (c) Reconstructed phase image obtained from the phase-retrieval algorithm after two iterations. (d) Reference image recorded using an optical microscope. (e) Estimated phase image at the sensor plane. The scale bar is approximately 1 mm.

In the second sample, the diffracted light illuminates on the basal area of an insect wing for phase imaging. Figure 3(a)-(e) shows recorded intensity image, rescaled intensity image, reconstructed phase image using GSA after four repeats, optical image, and the estimated phase image, respectively. As shown in figure 3(d) and (e), the veins are in colour blue due to NIR absorption. The phase variations can be observed within the transparent cell area, which is not visible in optical image. Thus, the reconstructed phase image can reveal the phase variation of the insect wing membrane.

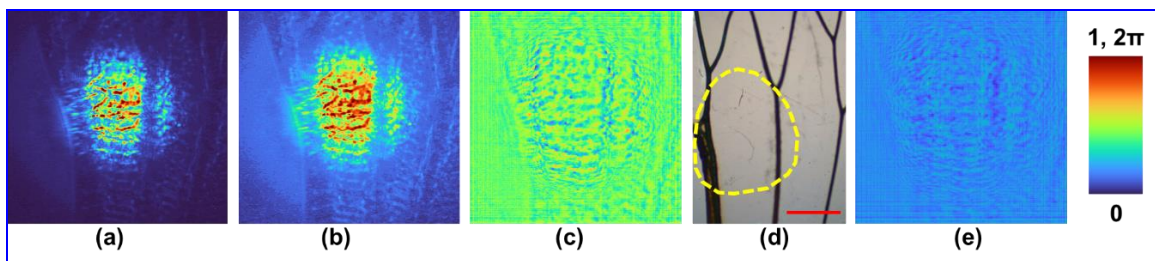


**Figure 3.** (a) Recorded intensity distribution for the wing sample taken from an insect. (b) Calculated amplitude of the recorded intensity distribution. (c) Reconstructed phase image obtained from the phase-retrieval algorithm after four iterations. (d) Reference image recorded using an optical microscope. (e) Estimated phase image at the sensor plane. The yellow dotted lines in (d) indicates the region of beam illumination. The scale bar is approximately 1 mm.

#### 4. CONCLUSION

The phase imaging of two biochemical samples has been achieved using synchrotron NIR source and fast phase-retrieval algorithm for the first time. However, this imaging method imposes a challenge that most of biochemical samples exhibit a strong absorption of NIR radiation and lower signals are detected at sensor plane. Although the detected intensity can be improved by using larger size pinholes, there is trade-off between spatial coherence and obtaining higher light throughput. This imaging technique can be integrated to the existing synchrotron measurement system of IRM beamline, which gives better understanding of the samples by measuring both functional and phase information simultaneously.

#### REFERENCES

- [1] Anand, V.; Ng, S.H.; Katkus, T.; Maksimovic, J.; Klein, A.; Vongsivut, J.; Bambery, K.; Tobin, M.J.; Juodkazis, S.; Exploiting spatio-spectral aberrations for rapid synchrotron infrared imaging. *J. Synchrotron. Rad.* **2021**, *28*, 1616-1619. <https://doi.org/10.1107/S1600577521007104>

- [2] Anand, V.; Han, M.; Maksimovic, J.; Ng, S.H.; Katkus, T.; Klein, A.; Bambery, K.; Tobin, M.J.; Vongsvivut, J.; Juodkazis, S. Single-shot mid-infrared incoherent holography using Lucy-Richardson-Rosen algorithm. *Opto-Electron. Sci.* **2022**, *1*, 210006. <https://doi.org/10.29026/oes.2022.210006>
- [3] Ryu, M.; Honda, R.; Balcytis, A.; Vongsvivut, J.; Tobin, M.J.; Juodkazis, S.; Morikawa, J. Hyperspectral mapping of anisotropy. *Nanoscale Horiz.* **2019**, *4*, 1443–1449. <https://doi.org/10.1039/C9NH00340A>
- [4] Ryu, M.; Linklater, D.; Hart, W.; Balčytis, A.; Skliutas, E.; Malinauskas, M.; Appadoo, D.; Tan, Y.R.E.; Ivanova, E.P.; Morikawa, J.; and Juodkazis, S. 3D printed polarizing grids for IR-THz synchrotron radiation. *J. Opt.* **2018**, *20*, 035101. <https://doi.org/10.1088/2040-8986/aaa6fb>
- [5] Praveen, P.A.; Arockiaraj, F.G.; Gopinath, S.; Smith, D.; Kahro, T.; Valdma, S.-M.; Bleahu, A.; Ng, S.H.; Reddy, A.N.K.; Katkus, T.; Rajeswary, A.S.J.F.; Ganeev, R.A.; Pikker, S.; Kukli, K.; Tamm, A.; Juodkazis, S.; Anand, V. Deep Deconvolution of Object Information Modulated by a Refractive Lens Using Lucy-Richardson-Rosen Algorithm. *Photonics* **2022**, *9*, 625. <https://doi.org/10.3390/photonics9090625>
- [6] Gerchberg, R. W.; Saxton, W. O.; A practical algorithm for the determination of phase from image and diffraction plane pictures. *Optik (Stuttg.)* 1972, *35*, 227–246.
- [7] Fienup, J.R. Phase retrieval algorithms: A comparison. *Appl. Opt.* **1982**, *21*, 2758–2769. <https://doi.org/10.1364/AO.21.002758>
- [8] Bauschke, H.H.; Combettes, P.L.; Luke, D.R. Phase retrieval, error reduction algorithm, and Fienup variants: A view from convex optimization. *J. Opt. Soc. Am. A* **2002**, *19*, 1334–1345. <https://doi.org/10.1364/JOSAA.19.001334>
- [9] Bao, P.; Zhang, F.; Pedrini, G.; Osten, W. Phase retrieval using multiple illumination wavelengths. *Opt. Lett.* **2008**, *33*, 309–311. <https://doi.org/10.1364/OL.33.000309>